water

MDPI

Article

Contribution of Biological Effects to the Carbon Sources/Sinks and the Trophic Status of the Ecosystem in the Changjiang (Yangtze) River Estuary Plume in Summer as Indicated by Net Ecosystem Production Variations

Yifan Zhang, Dewang Li, Kui Wang * and Bin Xue

Key Laboratory of Marine Ecosystem and Biogeochemistry, State Oceanic Administration & Second Institute of Oceanography, Ministry of Natural Resources, P.R. China, Hangzhou 310012, China; angela06z@163.com (Y.Z.); dwli@sio.org.cn (D.L.); xuebin119@sio.org.cn (B.X.)

* Correspondence: wangkui@sio.org.cn

Received: 6 May 2019; Accepted: 13 June 2019; Published: 17 June 2019

Abstract: We conducted 24-h real-time monitoring of temperature, salinity, dissolved oxygen, and nutrients in the near-shore (M4-1), front (M4-8), and offshore (M4-13) regions of the 31° N section of the Changjiang (Yangtze) River estuary plume in summer. Carbon dioxide partial pressure changes caused by biological processes (pCO_2bio) and net ecosystem production (NEP) were calculated using a mass balance model and used to determine the relative contribution of biological processes (including the release of CO_2 from organic matter degradation by microbes and CO_2 uptake by phytoplankton) to the CO_2 flux in the Changjiang River estuary plume. Results show that seawater in the near-shore region is a source of atmospheric CO_2, and the front and offshore regions generally serve as atmospheric CO_2 sinks. In the mixed layer of the three regions, pCO_2bio has an overall positive feedback effect on the air–sea CO_2 exchange flux. The contribution of biological processes to the air–sea CO_2 exchange flux (Cont) in the three regions changes to varying extents. From west to east, the daily means (±standard deviation) of the Cont are 32% (±40%), 34% (±216%), and 9% (±13%), respectively. In the front region, the Cont reaches values as high as 360%. Under the mixed layer, the daily means of potential Conts in the near-shore, front, and offshore regions are 34% (±43%), 8% (±13%), and 19% (±24%), respectively. The daily 24-hour means of NEP show that the near-shore region is a heterotrophic system, the front and offshore regions are autotrophic systems in the mixed layer, and all three regions are heterotrophic under the mixed layer.

Keywords: biological processes; air–sea CO_2 exchange flux; net ecosystem production; potential CO_2 emissions; trophic status; Changjiang River estuary plume

1. Introduction

The Changjiang estuary plume is a typical marginal sea with a coastal continental shelf that has large spatial and temporal variations in carbon sinks/sources. In summer, the East China Sea generally acts as a carbon sink for atmospheric CO_2 (-4.6 ± 1.3 mmol m^{-2} day^{-1}) [1–3]. The influence of physical processes, such as strong winds, and the large amount of dissolved inorganic carbon produced by respiration under the mixed layer turns the region into an atmospheric carbon source [4]. The water mass compositions in the mixed layer of the Changjiang River estuary plume are determined primarily by the Changjiang Diluted Water and the Kuroshio Surface Water. However, the originally deep (50 m) subsurface water of the Kuroshio [5] will rise and form an upwelling around 123° E, where

there is a trough [6]. On shorter time scales (e.g., 24-h), the complicated physical (upwelling, wind, tidal mixing, etc.) and biogeochemical (including the release of CO_2 from organic matter degradation by microbes and CO_2 uptake by phytoplankton) effects on the coastal and shelf ecosystems lead to complex transitions between carbon sinks and sources [7]. Thus, observations at high temporal resolutions are urgently needed to study the effects of biological processes on carbon sinks and sources.

The difference between gross primary production (GPP) and respiration (R) in an ecosystem is defined as the net ecosystem production (NEP) [8]. Negative NEP indicates that the ecosystem is heterotrophic, and positive NEP indicates that it is autotrophic; therefore, NEP can be used as an indicator of the trophic status, which is an important factor in the assessment of a specific ecosystem [9,10]. For example, Li [11] estimated the nutrient flux, primary production, and NEP in the Changjiang River estuary in the four seasons using the budget box model. Xu [12] used in situ sampling data and the "muddy" LOICZ (land–ocean interaction in the coastal zone) model to evaluate the tropical status of the Changjiang River estuary plume in summer and winter. NEP is also used to distinguish biogeochemical controls from other controls of carbon sinks and sources in marginal environments [13,14]. For instance, Borges established the relationship between mixed-layer NEP and air–sea CO_2 flux in order to detail the function of biogeochemical processes in European coastal seas [15]. Studies of NEP in the Changjiang River estuary plume have mostly applied the biogeochemical budget model on a seasonal scale. However, the contributions of biological processes to the impact of air–sea CO_2 flux using continuous monitoring data have rarely been reported. In addition, the quantification of potential CO_2 flux under the mixed layer using NEP remains to be studied in depth.

In this study, data from 24 hours of continuous monitoring in the Changjiang River estuary plume in summer were used to further explore these processes. The diel variations in parameters such as carbon dioxide partial pressure (pCO_2) and NEP in the near-shore, front, and offshore regions were calculated by a mass balance model to separate the controlling processes of pCO_2. We differentiated the air–sea CO_2 exchange flux associated with physical and biological processes and then quantified the contribution of biological processes to the total air–sea CO_2 exchange flux in the mixed layer. We also attempted to calculate the quantitative potential CO_2 emission under the mixed layer. Moreover, the NEP vales of the three regions were compared to assess the trophic statuses of the different ecosystems. The results demonstrate the importance of biological processes in the regulation of estuarine carbon sources and sinks, and they also show the gradients of trophic statuses that are influenced by Changjiang-diluted water in the Changjiang River estuary plume.

Our research on the carbon sinks and sources and assessment of the trophic statuses is based on a 24-h dataset. Although this maybe a shorter period than the timescale at which pCO_2 variation occurs in a carbonate system because of the buffer capacity of seawater, this study is meaningful from the perspective of the steady state over several months in summer in the Changjiang River estuary plume [16].

2. Materials and Methods

2.1. Study Area

Changjiang-diluted water has a strong influence on the Changjiang River estuary plume by virtue of a water discharge of about 944×10^9 m^{-3} $year^{-1}$ [17] that carries a large amount of nutrients and sediments [18]. The eutrophic Changjiang-diluted water enters the upper estuary area, resulting in phytoplankton blooms that can absorb a substantial quantity of atmospheric CO_2 [19]. At the same time, fluvial carbon input [20], as well as the decomposition and regeneration of organic matter in primary production, causes the estuary to release CO_2 into the atmosphere [21]. In addition, the Changjiang River estuary plume has a regular semidiurnal tide [22], which results in periodic changes in sea surface temperature and salinity. The largest monthly water discharge at Datong Station, which is 624 km from the river mouth, occurred in July, with the second largest occurring in August [23].

2.2. Sampling Collection

Samples from M4-1 (122.13° E, 31.04° N), M4-8 (122.97° E, 31° N), and M4-13 (124.01° E, 31° N) were collected on 26–27 July, 13–14 August, and 14–15 August in 2006 during cruises on the Changjiang River estuary plume (Figure 1). No tropical cyclones, typhoons, or rainstorms occurred during the sampling period [24]. Although the sampling period spanned nearly 17 days because the three stations are regulated by regular semidiel tides, we considered the water properties of each station to be quasisynchronized within almost one month, so each station is representative of a typical summer in a specific location. This is consistent with approaches used by other studies in summer [25–27]. The water depths at each station were 6, 52, and 37 m, respectively. Samples from the surface layer (2 m), depths of 5, 10, 30, and the bottom layer (with a height of 2 m above the seabed) were collected every three hours for 24 hours. In particular, we collected 5 m when the high slack tide impacted the M4-1 station and 4 m otherwise. In this study, M4-1, M4-8, and M4-13 denote the near-shore, front, and offshore regions, respectively.

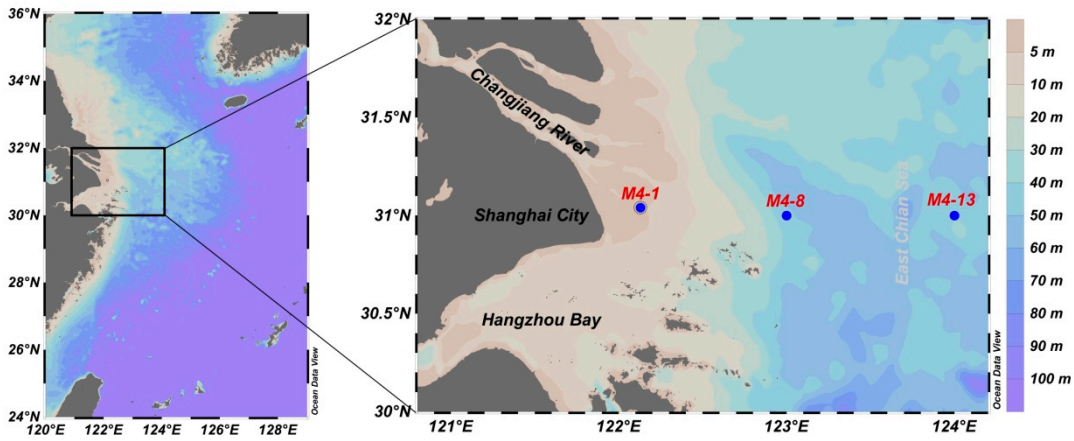

(**a**) (**b**)

Figure 1. Map of Changjiang River estuary plume (**a**) and sampling stations (**b**): stations M4-1, M4-8, and M4-13 denote the near-shore, front, and offshore regions, respectively.

2.3. Hydrographic Measurements

Seawater samples were collected using a rosette water collector. Temperature, salinity, and depth data were measured in situ with a Hydro-bios®MWS6 conductivity-temperature-depth (CTD) recorder. The data were recorded every three hours and monitored continuously for 24 hours. pH was measured with an ORION Ross-type combination electrode, which was calibrated on the NBS scale. The measurement precision was ±0.01 pH units. Total alkalinity (TA) was calculated using the TA–salinity relationship (equation 1), which was acquired by averaging the slopes and intercepts of the TA–salinity relationships in Table 1. The partial pressures of CO_2 (pCO_2) and dissolved inorganic carbon (DIC) were calculated from pH and TA using the program CO2SYS [28].

$$\text{TA } (\mu\text{mol kg}^{-1}) = (13.38 \pm 0.15)\text{S} + (1788.40 \pm 32.63) \quad (1)$$

Table 1. Summary of correlation between total alkalinity (TA, μmol kg^{-1}) and salinity.

Sampling Date	Sampling Area	Correlation	Reference
27 August 2013	31–31.5° N, 121.5–124° E (with a salinity of 5.17–34.26)	TA = 13.3507S + 1797.39	[7]
August 2009	31° N, 122.5–125° E (Transect C)	TA = 13.2S + 1744.7	[29]
8–27 April and 2–7 May 2007	30.0–31.8° N, 122.5–123.5° E (with a salinity of 13.00–34.49)	TA = 13.5875S + 1823.1	[30]

2.4. Mass Balance Model Based on Separating pCO_2-Controlling Processes

The volumetric flow equation [31] was used to calculate the air–sea CO_2 exchange flux:

$$F_{CO2} = k \times K_0 \times (pCO_{2water} - pCO_{2air}) \quad (2)$$

where pCO_{2air} and pCO_{2water} are the partial pressures of CO_2 in the atmosphere and surface water (μatm), respectively; pCO_{2air} was 380 and 377 μatm in July and August 2006, respectively (ftp://aftp.cmdl.noaa.gov/data/trace_gases/co2/flask/surface/co2_tap_surface-flask_1_ccgg_month.txt). F_{CO2} is the air–sea CO_2 exchange flux (mmol m^{-2} day^{-1}), where $F_{CO2} > 0$ indicates that seawater releases CO_2 into the atmosphere, and $F_{CO2} < 0$ means that seawater absorbs atmospheric CO_2. K_0 is the solubility coefficient of CO_2 in seawater [32], and k is the gas transfer velocity. For short-term wind, k was calculated using the empirical formula proposed by Wanninkhof [33] and revised by Sweeney [34]:

$$k = 0.27 \times U_{10}{}^2 \times (Sc/660)^{-0.5} \quad (3)$$

$$Sc = Sc_0 \times (1 + 3.14S/1000) \quad (4)$$

$$Sc_0 = 0.0476T^3 + 3.7818T^2 - 1.201T + 1800.6 \quad (5)$$

where U_{10} is the wind speed (m s^{-1}) at a height of 10 m above the sea surface (Remote Sensing Systems, CCMP Wind Vector Analysis Product, http://www.remss.com/measurements/ccmp/); Schmidt number (Sc) is expressed as a function of temperature (T, Celsius) and salinity (S, psu) [33,35].

We chose to use the mass balance method [36,37] that was modified for the calculation of NEP. At the initial time (t_1), the sea surface temperature (SST), sea surface salinity (SSS), and carbonate system parameters, including dissolved inorganic carbon (DIC), total alkalinity (TA), and pCO_2, are T_1, S_1, TA_1, DIC_1, and $(pCO_2)_1$, respectively. At time t_2, the above parameters are change to T_2, S_2, TA_2, DIC_2, and $(pCO_2)_2$.

$$\Delta pCO_2 = (pCO_2)_2 - (pCO_2)_1 = \Delta pCO_{2tem} + \Delta pCO_{2a\text{-}s} + \Delta pCO_{2mix} + \Delta pCO_{2bio} + \Delta pCO_{2non} \quad (6)$$

$$\Delta DIC = \Delta DIC_{a\text{-}s} + \Delta DIC_{mix} + \Delta DIC_{bio} \quad (7)$$

The subscripts "tem", "a-s", "mix", and "bio" of the specific parameter denote temperature, air–sea exchange, mixing, and in situ biological processes (including the release of CO_2 from organic matter degradation by microbes and CO_2 uptake by phytoplankton), respectively. "Δ" refers to the change in a particular parameter within a certain period of time (from t_1 to t_2). On a short timescale (three hours or each day), the nonlinear term (ΔpCO_{2non}) is essentially zero. The four different factors in Equation (6) were calculated as described below.

First, the thermal effect on ΔpCO_2 was calculated by Equation (8).

$$\Delta pCO_{2tem} = (pCO_2)_1 \times \exp(0.0423 \times (T_2 - T_1)) - (pCO_2)_1 \quad (8)$$

where 0.0423 is the temperature dependence coefficient of pCO_2 presented by Takahashi [38].

Second, air–sea CO_2 exchanges only change DIC and pCO_2 but have no effect on TA.

$$\Delta DIC_{a\text{-}s} = -F_{CO2} \times \Delta t/(\rho \times MLD) \quad (9)$$

$$(DIC_2)_{a\text{-}s} = DIC_1 + \Delta DIC_{a\text{-}s} \quad (10)$$

$$\Delta pCO_{2a\text{-}s} = f((DIC_2)_{a\text{-}s}, TA_1, S_1, T_1) - (pCO_2)_1 \quad (11)$$

where ρ is seawater density (kg m^{-3}), MLD is the mixed-layer depth, and $(DIC_2)_{a\text{-}s}$ is the DIC concentration at time t_2 and is affected only by the air–sea exchange from t_1 to t_2. The functions $f((DIC_2)_{a\text{-}s}, TA_1, S_1, T_1)$ were calculated using the CO2SYS program [28], and the dissociation constants

were taken from Dickson et al. [39].The evaluation of the mixed-layer depth (MLD) was based on the sigma-*t* criterion proposed by Sprintall [40], and it was calculated as follows:

$$\sigma_{t,MLD} = \sigma_{t,0} + \Delta T \times (\partial t/\partial T) \tag{12}$$

$$\sigma_t = \rho - 1000 \tag{13}$$

where $\sigma_{t,0}$ is the σ_t value in the surface layer. ΔT is the desired temperature difference, and $\Delta T = 0.5$ °C in this study. The coefficient of thermal expansion ($\partial t/\partial T$) was calculated from the surface temperature and salinity.

Third, using the interaction with the above-mentioned Kuroshio current, the original sources of the three end-member water masses were determined to be Changjiang diluted water (CDW), Kuroshio surface water (KSW), and Kuroshio subsurface water (KSSW) (Figure 2). The equations and characteristics of the three end-member mixing model are as follows (Table 2).

$$m_{CDW} + m_{KSW} + m_{KSSW} = 1 \tag{14}$$

$$m_{CDW} \times S_{CDW} + m_{KSW} \times S_{KSW} + m_{KSSW} \times S_{KSSW} = S \tag{15}$$

$$m_{CDW} \times \theta_{CDW} + m_{KSW} \times \theta_{KSW} + m_{KSSW} \times \theta_{KSSW} = \theta \tag{16}$$

where the subscripts CDW, KSW, and KSSW denote the three end-member water masses CDW, KSW, and KSSW, respectively; m_{CDW}, m_{KSW}, m_{KSSW} respectively denote the proportion of three end-members water masses; S_{CDW}, S_{KSW}, S_{KSSW} and θ_{CDW}, θ_{KSW}, θ_{KSSW} denote the salinity and bit temperature of the three-terminal element, respectively; S and θ denote the measured salinity and potential temperature, respectively. From this calculation, the theoretical values of total alkalinity $(TA_2)_{mix}$ and dissolved inorganic carbon $(DIC_2)_{mix}$ due to mixing during a given time period (from t_1 to t_2) can be determined. Further, ΔpCO_{2mix} can be calculated. The equations are

$$m_{CDW} \times (TA_2)_{CDW} + m_{KSW} \times (TA_2)_{KSW} + m_{KSSW} \times (TA_2)_{KSSW} = (TA_2)_{mix} \tag{17}$$

$$m_{CDW} \times (DIC_2)_{CDW} + m_{KSW} \times (DIC_2)_{KSW} + m_{KSSW} \times (DIC_2)_{KSSW} = (DIC_2)_{mix} \tag{18}$$

$$\Delta pCO_{2mix} = f((DIC_2)_{mix}, (TA_2)_{mix}, S_2, T_1) - (pCO_2)_1 \tag{19}$$

where $(TA_2)_{CDW}$, $(TA_2)_{KSW}$, $(TA_2)_{KSSW}$ and $(DIC_2)_{CDW}$, $(DIC_2)_{KSW}$, $(DIC_2)_{KSSW}$ denote the TA and DIC concentrations of the three end-member at time t_2, respectively.

Table 2. Three end-member characteristics of water mass from measurements obtained during cruises in July and August 2006.

Sampling Date	θ (°C)	S	TA (μmol kg^{-1})	DIC (μmol kg^{-1})
CDW	27.76 ± 0.20	7.88 ± 0.28	1898 ± 3.6	1863 ± 3.6
KSW	29.49 ± 0.10	33.22 ± 0.33	2232 ± 4.4	1808 ± 0.6
KSSW	19.48 ± 0.09	34.11 ± 0.05	2244 ± 0.6	2105 ± 13

Finally, the pCO_2 changes caused by biological processes (ΔpCO_{2bio}) were calculated from the other DIC changes. Thus,

$$\Delta DIC_{bio} = \Delta DIC - (\Delta DIC_{a\text{-}s} + \Delta DIC_{mix}) \tag{20}$$

$$(DIC_2)_{bio} = DIC_1 + \Delta DIC_{bio} \tag{21}$$

$$\Delta pCO_{2bio} = f((DIC_2)_{bio}, TA_1, S_1, T_1) - (pCO_2)_1 \tag{22}$$

where $(DIC_2)_{bio}$ is the theoretical value of DIC at time t_2 due to biological processes that occurred during a given time period (from t_1 to t_2).

According to the definition, the NEP calculation formula is

$$NEP = -\Delta DIC_{bio}/\Delta t \quad (23)$$

The NEP values in or under the mixed layer (mmol C m^{-2} day^{-1}) were calculated using the integral of the NEP over different water layers (mmol C m^{-3} day^{-1}).

Finally, we calculated the CO_2 flux caused by biological processes and its contribution to the air–sea CO_2 exchange flux as

$$F_{CO2bio} = k \times K_0 \times \Delta pCO_{2bio} \quad (24)$$

$$F_{CO2non\text{-}bio} = F_{CO2} - F_{CO2bio} \quad (25)$$

$$Cont = (F_{CO2bio}/F_{CO2}) \times 100\% \quad (26)$$

where F_{CO2bio} is the change in CO_2 flux caused by biological processes (mmol m^{-2} day^{-1}) and $F_{CO2non\text{-}bio}$ is the change in CO_2 flux caused by other processes. $F_{CO2bio} > 0$ indicates that biological processes, such as the degradation of organic matter by microorganisms, cause seawater to release CO_2. $F_{CO2bio} < 0$ indicates that biological processes, such as absorption of CO_2 by phytoplankton photosynthesis, cause seawater to absorb CO_2 from the atmosphere. Cont is the contribution of CO_2 flux changes caused by biological processes to the air–sea CO_2 exchange flux. Cont > 0 means that the variation in CO_2 caused by biological processes has the same direction as the variation in air–sea CO_2 exchange, which indicates a positive feedback progress; Cont < 0 indicates a negative feedback progress.

Under the mixed layer, potential pCO_2 and pCO_{2bio} were evaluated with the CO2SYS program using DIC_2, TA_2, S_2, T_2 and $(DIC_2)_{bio}$, TA_1, S_1, and T_1, respectively. $^*F_{CO2}$ and $^*F_{CO2bio}$ for each depth were calculated using Equations (1) and (23), and then the potential carbon flux ($^*F_{CO2}$) and the potential carbon flux caused by biological processes ($^*F_{CO2bio}$) in the three regions at each time point were integrated for the water layers beneath the MLD.

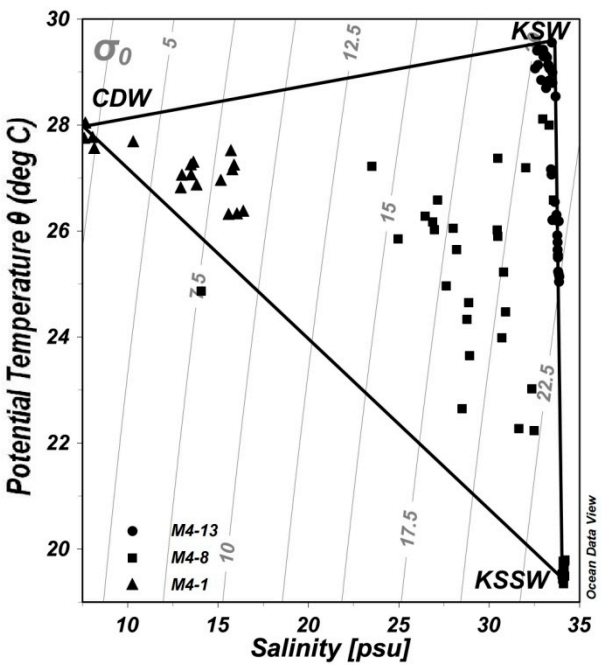

Figure 2. Scatter plots of potential temperature and salinity: M4-1 (triangles), M4-8 (squares), and M4-13 (circles). The labeled vertices denote the three end-members from the three water masses: Changjiang diluted water (CDW), Kuroshio surface water (KSW), and Kuroshio subsurface water (KSSW). Isoclines of potential density are shown in this figure.

2.5. Error Analysis

The uncertainty in pH arose from the pH measurement process. The uncertainty in TA is from the measured salinity and the TA–S Equation (1). The uncertainty in $(TA_2)_{mix}$ and $(DIC_2)_{mix}$ is introduced during the determination of the three endmembers. The uncertainty in DIC, pCO_{2water}, pCO_{2bio}, potential pCO_2, and pCO_{2bio} originates from CO2SYS with the equilibrium constants established by Mehrbach et al. [41] and refit by Dickson and Millero [39] (i.e., with carbonic acid dissociation constants omitted from calculations). The uncertainty in F_{CO2}, F_{CO2bio}, $^*F_{CO2}$, and $^*F_{CO2bio}$ arises from the calculation using the daily gas transfer velocity (k) and deviations in pCO_{2water} and pCO_{2bio}. In this study, we used error propagation formulas to estimate the uncertainties [42].

Assuming that the errors of the variables X, Y, and Z are δX, δY, and δZ, respectively, for linear sum functions, the error of R is

$$R = X + Y + Z \tag{27}$$

$$\delta R = \delta X + \delta Y + \delta Z \tag{28}$$

For multiplication and division, the error of R is

$$R = (X \times Y)/Z \tag{29}$$

$$(\delta R/R)^2 = (\delta X/X)^2 + (\delta Y/Y)^2 + (\delta Z/Z)^2 \tag{30}$$

Overall, the uncertainty in the salinity-based TA calculation is less than 3%; the uncertainties in $(TA_2)_{mix}$ and $(DIC_2)_{mix}$ are ~0.4% and ~0.8%, respectively; the uncertainty in k is ~13%; the uncertainty of F_{CO2}, F_{CO2bio}, $^*F_{CO2}$, and $^*F_{CO2bio}$ is ±1.61, ±2.10, ±2.61, and ±0.86 mmol m^{-2} day^{-1}, respectively.

3. Results

3.1. 24 Hourly Variations in Temperature and Salinity

The trend of the surface temperature in the three regions was offshore > near-shore > front, and the bottom temperature showed a trend of near-shore > offshore > front (Figure 3a–c). The trend of salinity in the surface and bottom layer showed a distribution trend of offshore > front > near-shore (Figure 3d–f). The difference between the surface and bottom temperature in the front region was the largest, followed by the offshore region, and the temperature difference in the near-shore region was the smallest. The temperature and salinity changes in the near-shore region fluctuated with a semidiurnal frequency. The temperature and salinity at 06:00 and 18:00 both had extreme values (Figure 3a,d). The relative standard deviation of surface salinity changes was as high as 25.82% in 24 hours. In the front region, the relative standard deviation of the temperature variation at 10 m reached 8.90%, and the salinity variation at 5 m was as high as 21.01%. In the offshore region, the temperature and salinity changes were small in 24 hours: the relative standard deviation of the temperature at 10 m was 5.15%, and the relative standard deviation of the changes in salinity at the surface in 24 hours was 1.01%; the others were less than 1%.

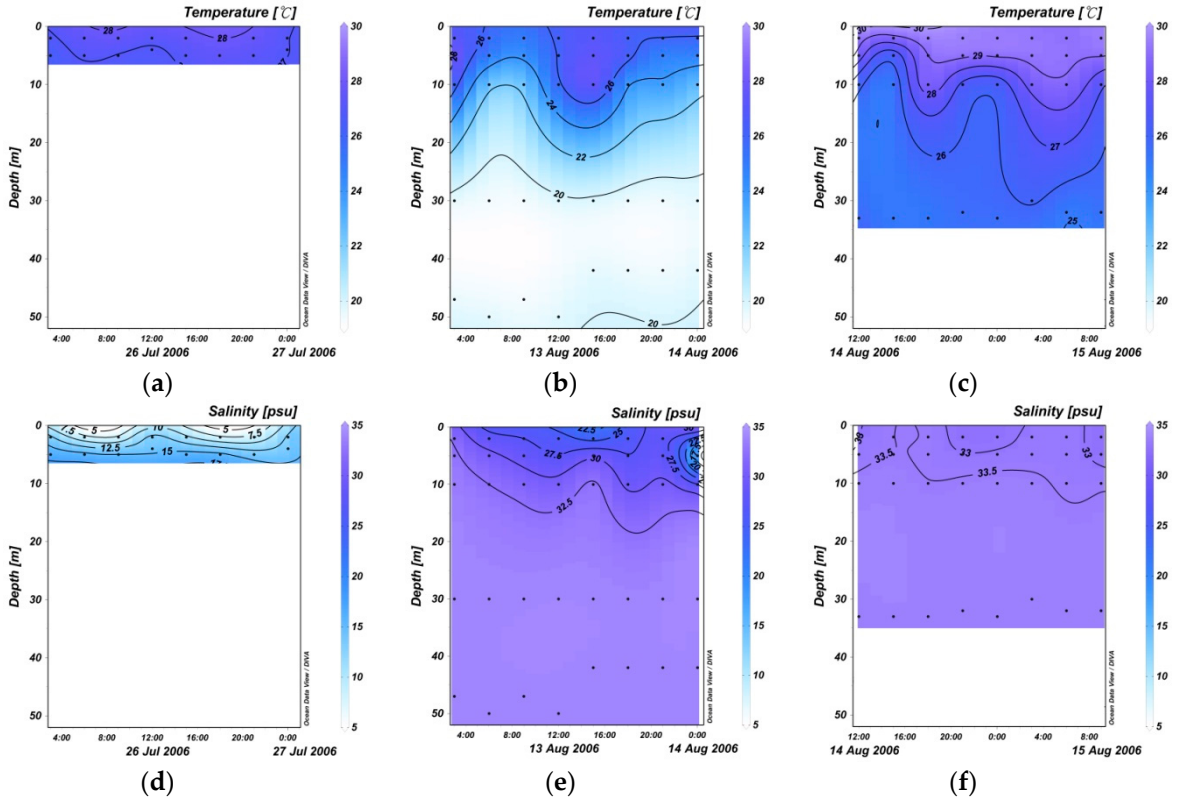

Figure 3. Twenty-four-hour variations in temperature in the near-shore (**a**), front (**b**), and offshore (**c**) regions and salinity in the near-shore (**d**), front (**e**), and offshore (**f**) regions in summer.

3.2. Variation in pH, TA, DIC, and Sea Surface pCO_2 within 24 Hours

In the near-shore region, the surface daily averages (standard deviations in brackets) of pH increased from 7.92 (±0.02) to 7.95 (±0.02) at the bottom (Figure 4a), TA increased from 1936.06 (±40.21) to 1993.43 (±15.01) μmol kg^{-1} at the bottom (Figure 4d), DIC increased from 1889.75 (±28.04) to 1919.82 (±9.35) μmol kg^{-1} at the bottom (Figure 4g), and pCO_2 decreased from 996 (±71) to 868 (±53) μatm at the bottom (Figure 4j).

In the front region, the surface daily averages (standard deviations in brackets) of pH decreased from 8.33 (±0.11) to 7.94 (±0.03) at the bottom (Figure 4b). TA increased from 2157.80 (±34.17) to 2244.12 (±0.68) μmol kg^{-1} at 30 m and then decreased to 2244.06 (±0.50) μmol kg^{-1} at the bottom (Figure 4e). DIC increased from 1833.97 (±68.63) to 2102.68 (±12.88) μmol kg^{-1} at the bottom (Figure 4h), and pCO_2 increased from 283 (±87) to 735 (±59) μatm at the bottom (Figure 4k).

In the offshore region, the surface daily averages (standard deviations in brackets) of pH decreased from 8.38 (±0.03) to 8.05 (±0.02) at the bottom (Figure 4c), TA increased from 2229.48 (±4.72) to 2240.15 (±0.53) μmol kg^{-1} at the bottom (Figure 4f), and DIC increased from 1791.73 (±24.87) to 2018.65 (±13.21) μmol kg^{-1} at the bottom (Figure 4i). Daily average pCO_2 was 227 (±23) μatm at the surface, and it decreased to 226 (±32) μatm at 5 m and then increased to 566 (±38) μatm at the bottom (Figure 4l).

Overall, from the vertical distribution of the water column, pH was generally highest at the surface and lowest at the bottom. On the contrary, TA, DIC, and pCO_2 were generally lowest at the surface and highest at the bottom. Spatially, pH and TA generally increased from the near-shore to the offshore region. On the contrary, DIC and pCO_2 generally decreased from the near-shore to the offshore region.

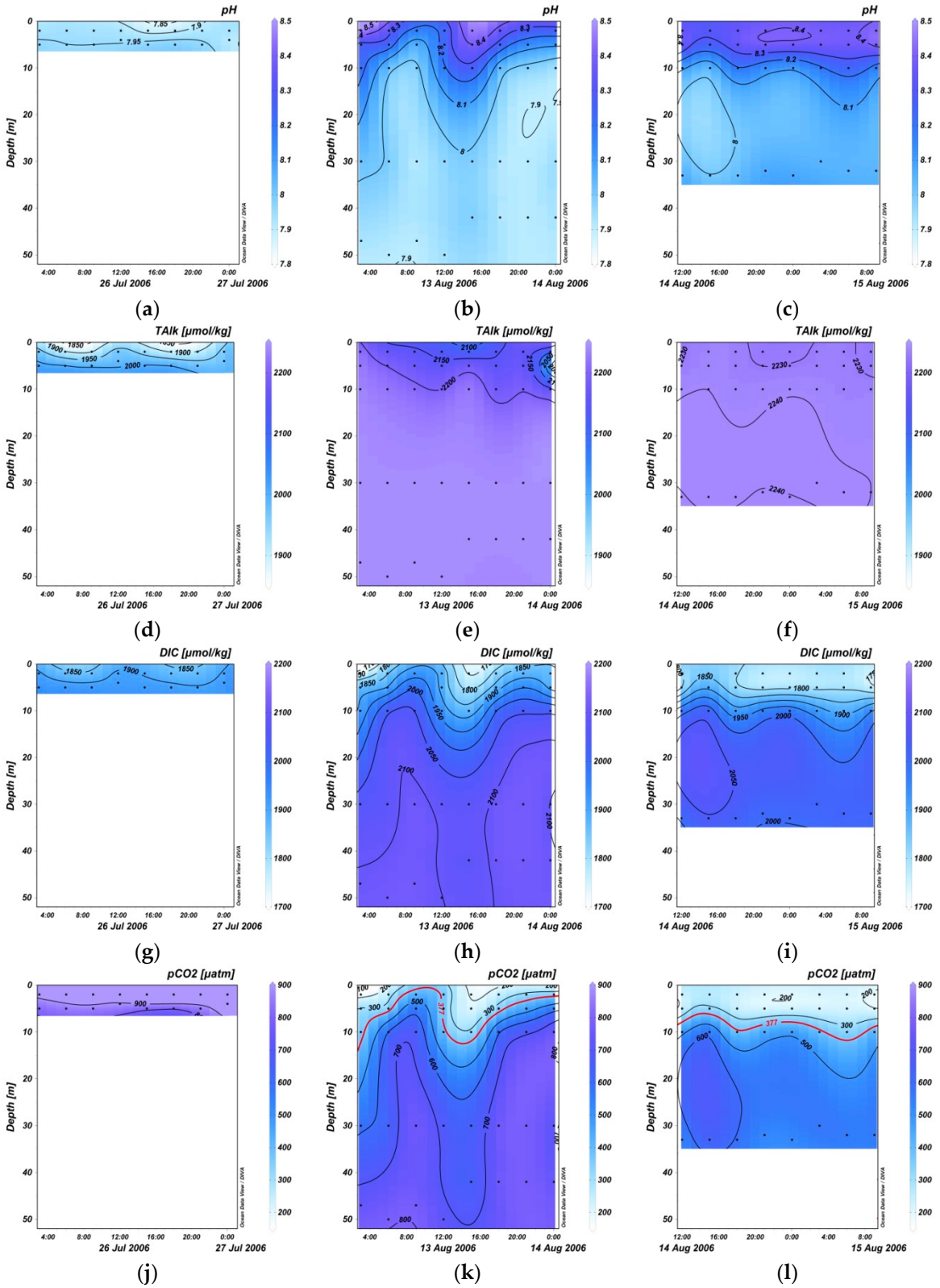

Figure 4. Twenty-four hour variations in pH in the near-shore (**a**), front (**b**), and offshore (**c**) regions; TA in the near-shore (**d**), front (**e**), and offshore (**f**) regions; DIC in the near-shore (**g**), front (**h**), and offshore (**i**) regions; and sea surface pCO_2 in the near-shore (**j**), front (**k**), and offshore (**l**) regions in summer.

3.3. Variation in NEP within 24 Hours

In the near-shore region, there were negative NEP values, and the NEP at the bottom was slightly larger than that at the surface (Table 3). The minimum NEP value was −0.36 mmol C m^{-3} day^{-1} at 12:00 at the surface, and the maximum value was 0.13 mmol C m^{-3} day^{-1} at 15:00 at the bottom (Figure 5a).

Table 3. Minimum, maximum, mean, and standard deviation of NEP in the three regions in summer (mmol C m^{-3} day^{-1}).

Regions	Depth	Minimum	Maximum	Mean	Standard Deviation
Near-shore	Surface	−0.36	0.09	−0.12	0.16
	Bottom	−0.34	0.13	−0.17	0.18
Front	Surface	−0.04	1.89	1.07	0.62
	5 m	0.19	1.26	0.65	0.38
	10 m	−0.32	0.28	−0.05	0.20
	30 m	−0.15	0.21	−0.01	0.12
	Bottom	−0.16	0.11	−0.08	0.09
Offshore	Surface	−0.14	0.43	0.16	0.19
	5 m	−0.08	0.52	0.22	0.17
	10 m	−0.54	0.28	−0.08	0.31
	Bottom	−0.31	0.03	−0.09	0.12

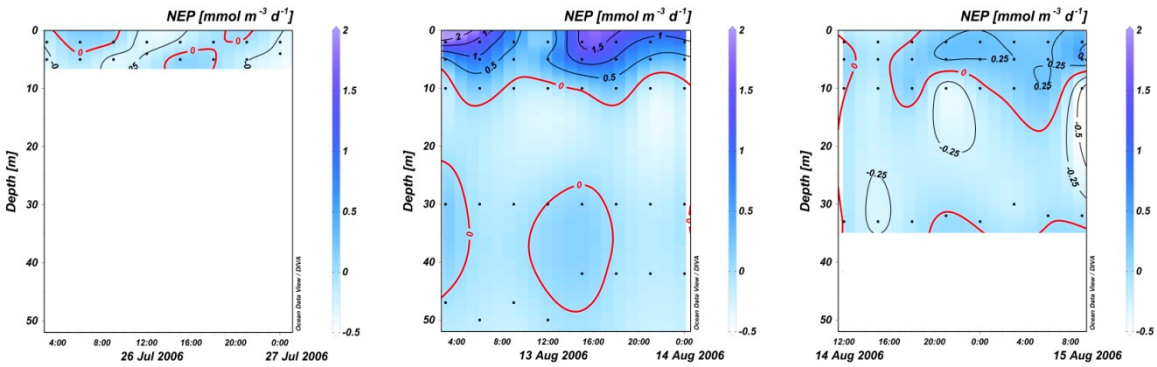

(**a**) (**b**) (**c**)

Figure 5. Twenty-four-hour variation in NEP in the near-shore (**a**), front (**b**), and offshore (**c**) regions in summer.

In the front region, the maximum NEP value (1.89 mmol C m^{-3} day^{-1}) was observed at 03:00 at the surface, and the minimum value (−0.32 mmol C m^{-3} day^{-1}) was observed at 21:00 at 10 m (Figure 5b). In the vertical direction, the daily variation in the surface NEP was slightly larger than that at the bottom. In the front region, the daily mean NEP from the surface to the bottom generally decreased, and the 24-h variation in NEP in the mixed layer (Table 3) was larger than that under the mixed layer (Table 4).

Table 4. Mixed layer depth (m) at each measurement time within 24-h in three regions.

Regions	00:00	03:00	06:00	09:00	12:00	15:00	18:00	21:00
Near-shore	2.73	2.14	2.06	2.06	2.72	2.09	2.06	2.09
Front	8.49	2.94	2.18	2.36	2.83	2.07	5.11	2.35
Offshore	3.29	6.03	8.84	5.03	3.05	2.45	6.67	3.44

In the offshore region, the maximum NEP (0.52 mmol C m^{-3} day^{-1}) was observed at 09:00 at 5 m, while the minimum NRP (−0.54 mmol C m^{-3} day^{-1}) was observed at 10 m (Figure 5c). The largest variation in NEP within 24-h was at 10 m, and the smallest variation was at the bottom (Table 3).

4. Discussion

4.1. Variations in F_{CO2bio} and F_{CO2} in the Mixed Layer

F_{CO2} is strongly positive in each timeslot (Figure 6a), indicating that this region acts as a source of atmospheric CO_2 [43,44] because the near-shore region is affected by the CDW [45] which has abundant pCO_2 [25,26]. F_{CO2bio} is strongly positive most of the time (Figure 6a), meaning that heterotrophic respiration releases CO_2 to the atmosphere for most of the day in the near-shore region. Because this study region is located in the largest turbid zone of the Changjiang River estuary plume [46,47], we infer that the mixing effect and extremely limited light may reduce the primary production by phytoplankton photosynthesis and that planktonic community respiration may dominate the biological processes, which maintain a high pCO_2 value in the near-shore region.

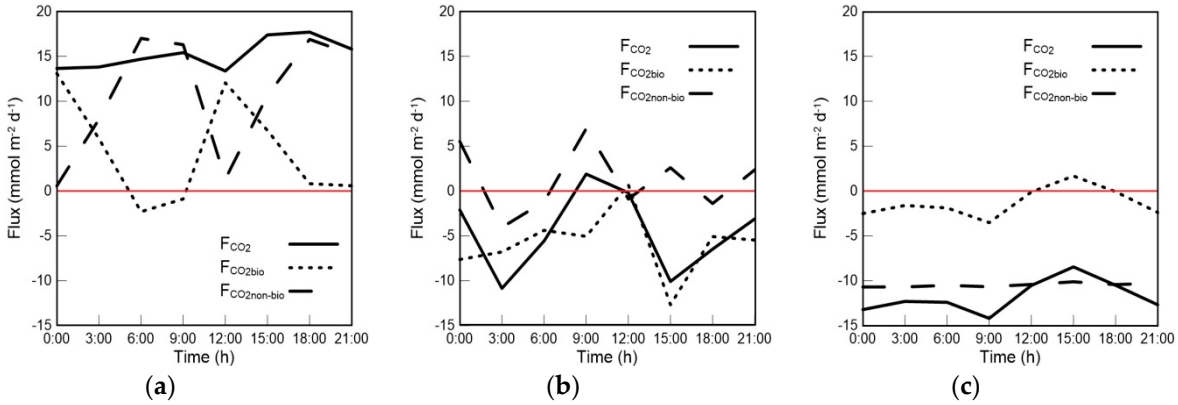

Figure 6. Twenty-four hour variations in F_{CO2}, F_{CO2bio}, and $F_{CO2non\text{-}bio}$ in the near-shore (**a**), front (**b**), and offshore (**c**) regions in summer.

The 24-h F_{CO2} in the front region is almost negative (Figure 6b), indicating that the front region acts as a sink for atmospheric CO_2. The 24-h F_{CO2bio} in the front region is also almost negative which indicates the biological processes absorb CO_2 (Figure 6b). Because of the high values of NEP (Figure 5b, Table 3) and Chl *a* [6] in this region, we infer that the front region has a great capacity for biological productivity and that a large amount of CO_2 is fixed in the surface water by phytoplankton.

Most F_{CO2} values in the offshore region are mostly slightly less than 0 (Figure 6c), indicating that the offshore region acts as a sink for atmospheric CO_2. This finding is in agreement with the study by Song et al. [2]. F_{CO2bio} in the offshore region was mostly slightly less than 0 (Figure 6c), indicating that the photosynthesis rate of fixed CO_2 by phytoplankton is higher than degradation rates of organic matter releasing CO_2 by microbial action in the offshore region.

4.2. The Contribution of Biological Processes to the Air–Sea CO_2 Exchange Flux in the Mixed Layer

F_{CO2} in the mixed layer of the three regions shows that the near-shore region acts as a strong source of atmospheric CO_2 (Figure 6a) and that the front and offshore regions act as sinks for atmospheric CO_2 (Figure 6b,c), similar to the results of other studies [1,48,49]. The daily average Cont in the mixed layer shows that the biological processes have a positive feedback effect on air–sea CO_2 exchange in the near-shore, front, and offshore regions (Table 5). This agrees with the conclusion of Borges et al. [15]. The air–sea CO_2 flux is inversely proportional to the NEP in the mixed layer, indicating that the contribution to the variation in air–sea CO_2 flux in these coastal waters is dominated by biological processes during a diel cycle. However, the average Cont in the offshore region is lower than that in the near-shore and front regions. This could be related to the fact that primary production in the offshore region is very low, even in summer, and other effects such as wind, temperature, and water mixing may play more important roles in controlling air–sea CO_2 flux.

Table 5. The contribution of CO_2 flux variation caused by biological processes to F_{CO2} (Cont) in the mixed layer.

Regions	00:00	03:00	06:00	09:00	12:00	15:00	18:00	21:00	Mean
Near-shore	96%	42%	−16%	−6%	90%	39%	5%	4%	32%
Front	360%	63%	79%	−269%	−341%	126%	78%	175%	34%
Offshore	19%	13%	15%	25%	1%	−20%	1%	19%	9%

4.3. Potential Carbon Sources under the Mixed Layer

Under the mixed layer (Table 4), the water column is determined to be a potential carbon source of atmospheric CO_2 in the three regions (Figure 7a–c). The variations in $*F_{CO2}$ and $*F_{CO2bio}$ show that the near-shore, front, and offshore regions could be potential atmospheric carbon sources, and a large amount of CO_2 produced by biological processes (e.g., respiration) is stored under the mixed layer (Figure 7). Although the surface water in the front and offshore regions acts as a sink for atmospheric CO_2, respiration under the mixed layer will result in the degradation of organic matter with substantial CO_2 release, which could be observed when vertical mixing occurred [27]. Hence, the CO_2 sink region in the Changjiang River estuary plume will become a source region when there is a tropical storm or an upwelling process. In a relevant study of the East China Sea, Chen et al. [4] also proposed that phytoplankton and planktonic bacteria could store dissolved inorganic carbon in the subsurface and might affect the surface air–sea CO_2 flux. Further, the daily means (standard deviations in brackets) of the potential contribution of biological processes to air–sea CO_2 exchange flux in the near-shore, front, and offshore regions are 34% (±43%), 8% (±13%), and 19% (±24%) in 24 hours, respectively, indicating that local respiration accounts for a large part of the total potential CO_2 release under the mixed layer. Other factors probably include KSSW intrusion, temperature elevation, and so on, which need further exploration.

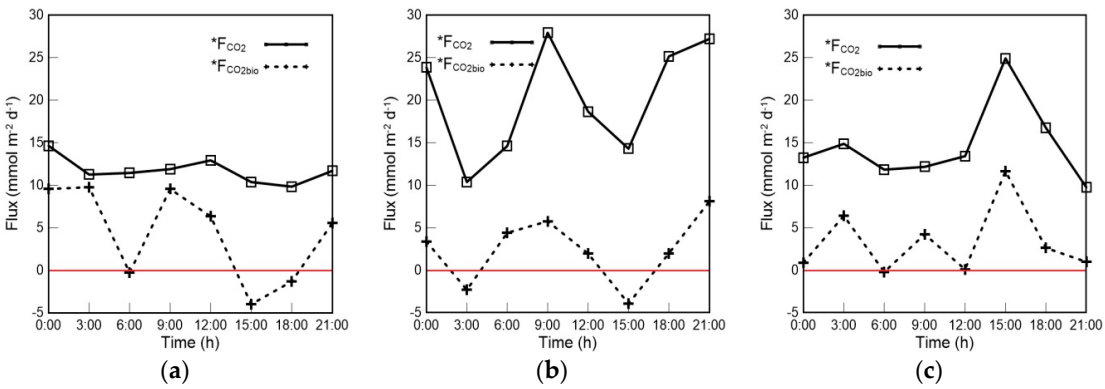

Figure 7. Twenty-four-hour variations in potential carbon flux ($*F_{CO2}$) and the biological contribution to carbon flux ($*F_{CO2bio}$) in the near-shore (**a**), front (**b**), and offshore (**c**) regions in summer.

4.4. Trophic Status Assessments and the Relationship between Cont and NEP

The mixed layer in the front and offshore regions is an autotrophic system (Table 3), but that in the near-shore region is a heterotrophic system. On the whole, we consider the Changjiang River estuary plume to be an autotrophic ecosystem in summer, similar to the conclusion of Li et al. [11], in August 2006. The daily mean NEP values of the study region are negative under the mixed layer, indicating that they are heterotrophic systems, which is in agreement with Chou et al. [27]. However, the positivity or negativity of the NEP values changes throughout a 24-hour period, and the trophic status of the same region varies as well. The Changjiang River estuary plume has a complex current structure featuring multiple eddies [50] or low salinity water detachment (LSW) [16]; however, eddies and LSW are on the mesoscale in terms of time and space (e.g., a couple of weeks and hundreds

of kilometers). In 24 hours, eddies and LSW have little effect on the variation in water properties. Therefore, we suggest that trophic statuses in a day are regulated by the tide.

In order to explore the influences of trophic status on Cont, we compared the Cont and NEP in the mixed layer in the region (Figure 8). The significant correlations between Cont and NEP in the mixed layer in the near-shore and offshore regions show that trophic status can be used as an index of the contribution of biological process to the air–sea CO_2 flux. Cont in the near-shore region has a significantly negative correlation ($r^2 = 0.94$, $p < 0.05$) with NEP, indicating that the more heterotrophic the system, the greater the influence on the contribution of biological processes (e.g., organic matter degradation by microorganisms) to F_{CO2}. When there is no biological contribution to F_{CO2} (Cont = 0), the NEP background value is −0.003 mmol C m^{-3} day^{-1}. In the front region, the correlation between Cont and NEP is not significant (Figure 8c). This could be because there are opposing processes causing the trophic status on the east and west sides of the front region, the west side of the front region is dominated by the degradation of organic matter, while the east side is dominated by the absorption of dissolved inorganic carbon. When the tide has a continuous impact on the front region, the NEP in the front region would present a large fluctuation. The NEP of offshore region was significantly and positively correlated with Cont ($r^2 = 0.94$, $p < 0.05$), indicating that the more autotrophic the system, the greater the contribution of the biological processes (e.g., primary production) to F_{CO2}. Assuming that there are no biological processes in the offshore region (Cont = 0), the background value of NEP was also 0.03 mmol C m^{-3} day^{-1} (Figure 8c). In addition, the slopes of NEP and Cont show that the biological processes have a stronger influence on the variation in the air–sea CO_2 exchange flux in the near-shore region than that in the offshore region when the two systems have an equal trophic status level.

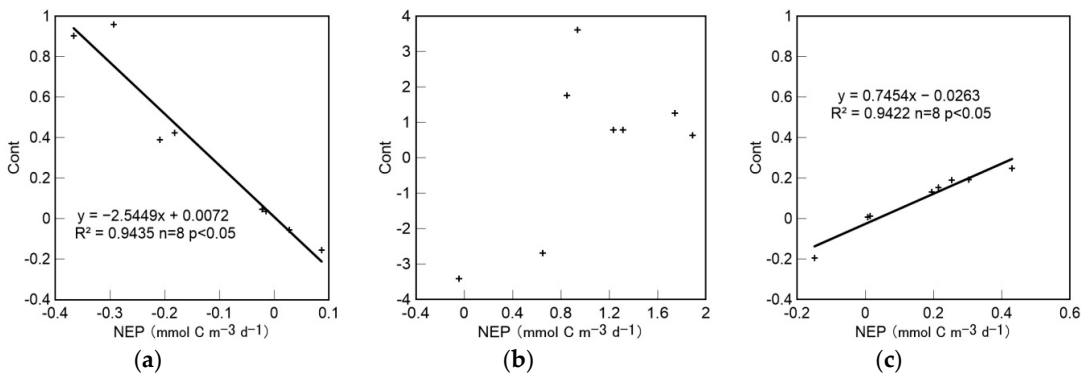

Figure 8. Correlations between Cont and NEP in the near-shore (**a**), front (**b**), and offshore (**c**) regions in the mixed layer in summer.

5. Conclusions

Using a mass balance model, we calculated the NEP, F_{CO2bio}, and F_{CO2} at eight time-points per day in the near-shore, front, and offshore regions of the Changjiang River estuary plume in summer. Then, we calculated the contribution of biological processes to F_{CO2} in the three regions. In the mixed layer, both F_{CO2} and F_{CO2bio} significantly varied at different times within the 24-h period. The near-shore region was found to be a source of atmospheric CO_2, and the offshore region is a sink for atmospheric CO_2. The front region is a sink for atmospheric CO_2 on the whole, but it transforms between a source and a sink from time to time. The biological processes in the mixed layer in the three regions were shown to have an overall positive feedback effect on the variation in the air–sea CO_2 exchange flux. Within the 24 hour period, the mean values of F_{CO2} and F_{CO2bio} were both positive in the near-shore region, indicating that CO_2 was being released into the atmosphere, and microbial degradation of organic matter accounted for a large part of this. In the front and offshore regions, the daily mean values of F_{CO2} and F_{CO2bio} were both negative, indicating that these areas absorb CO_2 from the atmosphere and that phytoplankton also fixes CO_2 from the atmosphere into the ocean. The daily averages of Cont

of stations from west to east were 32% (±40%), 34% (±216%), and 9% (±13%), respectively. Cont reached 360% in the front region. Under the mixed layer, the near-shore, front, and offshore regions could be potential carbon sources for the atmosphere. Therefore, the CO_2 sink region might become a source when there is a tropical storm or upwelling process that overturns the water from the deep. Under the mixed layer, the daily means of the potential contribution of biological processes to air–sea CO_2 exchange flux were 34% (±43%), 8% (±13%), and 19% (±24%) within the 24-h period, respectively. In addition, in the mixed layer, the near-shore region was shown to be a typical heterotrophic system, while the front and offshore regions are both autotrophic systems. Conversely, in all three regions, under the mixed layer is heterotrophic. However, at different time points, the trophic statuses change, even in the same region.

At a short timescale or in a steady-state environment, these conclusions can accurately represent the influence of biological processes on the variation in air–sea CO_2 exchange flux and can be used to assess the trophic statuses in the Changjiang River estuary plume in summer. Nevertheless, the biochemical and hydrological conditions in coastal regions constantly change at high frequency; thus, the use of data with high spatial and temporal resolutions is necessary to study the contribution of biological processes to the air–sea CO_2 exchange flux and to more accurately quantify the potential carbon stock of deep water bodies. Further, variations in long-term trophic statuses require additional exploration, especially in coastal waters, given the intensity of human activities and quickly progressing climate change.

Author Contributions: Conceptualization, Y.Z. and K.W.; Formal analysis, Y.Z. and D.L.; Investigation, K.W. and B.X.; Writing–original draft, Y.Z.; Writing–review & editing, D.L. and K.W.

Funding: This study was jointly supported by the National Natural Science Foundation of China (U1609201, U1709201, 91128212, 41203085, and 41206085), the Public Science and Technology Research Funds Projects of Ocean (201105014 and 201205015), the Scientific Research Fund of the Second Institute of Oceanography, State Oceanic Administration, China (JT1603), the Natural Science Project of Zhejiang Province (Y5110171,LQ17D060006), and the Project of State Key Laboratory of Satellite Ocean Environment Dynamics, Second Institute of Oceanography (SOEDZZ1402 and SOEDZZ1521).

Acknowledgments: The authors would like to thank the crew of R/V "China Marine Surveillance 49" for their supports in sampling and logistics. We also thank Wei-jun Cai (University of Delaware), Zhaohui Aleck Wang (Woods Hole Oceanographic Institution), Quanzhen Chen and his group, Daji Huang and his group, Jianfang Chen, Bin Wang and Tianzhen Zhang (Second Institute of Oceanography, Ministry of Natural Resources) for their technical support and helpful comments.

Conflicts of Interest: The authors declare no conflict of interest.

References

1. Guo, X.; Zhai, W.; Dai, M.; Zhang, C.; Bai, Y.; Xu, Y.; Li, Q.; Wang, G. Air–Sea CO_2 fluxes in the East China Sea based on multiple-year underway observations. *Biogeosciences* **2015**, *12*, 5123–5167. [CrossRef]
2. Song, J.; Qu, B.; Li, X.; Yuan, H.; Li, N.; Duan, L. Carbon sinks/sources in the Yellow and East China Seas—Air-sea interface exchange, dissolution in seawater, and burial in sediments. *Sci. China Earth Sci.* **2018**, *61*, 1583. [CrossRef]
3. Jiao, N.; Liang, Y.; Zhang, Y.; Liu, J.; Zhang, Y.; Zhang, R.; Zhao, M.; Dai, M.; Gao, K.; Song, J.; et al. Carbon pools and fluxes in the China Seas and adjacent oceans. *Sci. China Earth Sci.* **2018**, *61*, 1535. [CrossRef]
4. Chen, C.; Chiang, K.; Gong, G.; Shiah, F.; Tseng, C.; Liu, K. Importance of planktonic community respiration on the carbon balance of the East China Sea in summer. *Glob. Biogeochem. Cycles* **2006**, *20*. [CrossRef]
5. Chen, C.A. The Kuroshio intermediate water is the major source of nutrients on the East China Sea continental shelf. *Oceanol. Acta* **1996**, *19*, 523–527.
6. Wang, K.; Chen, J.; Jin, H.; Gao, S.; Xu, J.; Lu, Y.; Haung, D.; Hao, Q.; Weng, H. Summer nutrient dynamics and biological carbon uptake rate in the Changjiang River plume inferred using a three end-member mixing model. *Cont. Shelf Res.* **2014**, *91*, 192–200. [CrossRef]
7. Li, D.; Chen, J.; Ni, X.; Wang, K.; Zeng, D.; Wang, B.; Jin, H.; Haung, D.; Cai, W. Effects of biological production and vertical mixing on sea surface pCO_2 variations in the Changjiang River plume during early autumn: A buoy-based time series study. *J. Geophys. Res. Ocean.* **2018**, *123*, 6156–6173. [CrossRef]

8. Odum, H.T. Primary production in flowing waters. *Limnol. Oceanogr.* **1956**, *1*, 102–117. [CrossRef]
9. Oviatt, C.A.; Doering, P.H.; Nowicki, B.L.; Zoppini, A. Net system production in coastal waters as a function of eutrophication, seasonality and benthic macrofaunal abundance. *Estuaries* **1993**, *16*, 247–254. [CrossRef]
10. Carvalho, M.C.; Schulz, K.G.; Eyre, B.D. Respiration of new and old carbon in the surface ocean: Implications for estimates of global oceanic gross primary productivity. *Glob. Biogeochem. Cycles* **2017**, *31*, 975–984. [CrossRef]
11. Li, X.; Yu, Z.; Song, X.; Cao, X.; Yuan, Y. Nitrogen and phosphorus budgets of the Changjiang River estuary. *Chin. J. Oceanol. Limnol.* **2011**, *29*, 762–774. [CrossRef]
12. Xu, H.; Wolanski, E.; Chen, Z. Suspended particulate matter affects the nutrient budget of turbid estuaries: Modification of the LOICZ model and application to the Yangtze Estuary. *Estuar. Coast. Shelf Sci.* **2013**, *127*, 59–62. [CrossRef]
13. Swaney, D.P.; Howarth, R.W.; Butler, T.J. A novel approach for estimating ecosystem production and respiration in estuaries: Application to the oligohaline and mesohaline Hudson River. *Limnol. Oceanogr.* **1999**, *44*, 1509–1521. [CrossRef]
14. Palevsky, H.I.; Quay, P.D. Influence of biological carbon export on ocean carbon uptake over the annual cycle across the North Pacific Ocean. *Glob. Biogeochem. Cycles* **2017**, *31*, 81–95. [CrossRef]
15. Borges, A.; Schiettecatte, L.-S.; Abril, G.; Delille, B.; Gazeau, F. Carbon dioxide in European coastal waters. *Estuar. Coast. Shelf Sci.* **2006**, *70*, 375–387. [CrossRef]
16. Xuan, J.; Huang, D.; Zhou, F.; Zhu, X.; Fan, X.; Ni, X.; Xing, C. Application of data assimilation to synoptic temperature mapping of the coastal ocean survey. *Oceanol. Limnol. Sin.* **2012**, *43*, 17–26.
17. Dai, A.; Trenberth, K.E. Estimates of freshwater discharge from continents: Latitudinal and seasonal variations. *J. Hydrometeorol.* **2002**, *3*, 660–687. [CrossRef]
18. Liu, X.C. Concentration variation and flux estimation of dissolved inorganic nutrient from the Changjianag River into its estuary. *Oceanol. Limnol. Sin.* **2002**, *32*, 332–340.
19. Wang, K.; Chen, J.; Ni, X.; Zeng, D.; Li, D.; Jin, H.; Glibert, P.; Qiu, W.; Haung, D. Real-time monitoring of nutrients in the Changjiang Estuary reveals short-term nutrient-algal bloom dynamics. *J. Geophys. Res. Ocean.* **2017**, *122*, 5390–5403. [CrossRef]
20. Liu, Q.; Guo, X.; Yin, Z.; Zhou, K.; Roberts, E.; Dai, M. Carbon fluxes in the China Seas: An overview and perspective. *Sci. China* **2018**, *61*, 1564–1582. [CrossRef]
21. Chen, C.; Shiah, F.; Chiang, K.; Gong, G.; Kemp, W. Effects of the Changjiang (Yangtze) River discharge on planktonic community respiration in the East China Sea. *J. Geophys. Res. Ocean.* **2009**, *114*. [CrossRef]
22. Huang, H.; Wang, Y.; Zhang, W. Characteristics of tidal waves in the eastern Jiangsu coast and Changjiang Estuary. In Proceedings of the 2015 International Forum on Energy, Environment Science and Materials, Shenzhen, China, 25–26 September 2015.
23. Chen, C.A.; Zhai, W.; Dai, M. Riverine input and air-sea CO_2 exchanges near the Changjiang (Yangtze River) Estuary: Status quo and implication on possible future changes in metabolic status. *Cont. Shelf Res.* **2008**, *28*, 1476–1482. [CrossRef]
24. Zhejiang Meteorological Bureau. *Zhejiang Provincial Climate Bulletin*; Zhejiang Meteorological Bureau: Zhejiang, China, 2006.
25. Zhai, W.; Dai, M. On the seasonal variation of air-sea CO_2 fluxes in the outer Changjiang (Yangtze River) Estuary, East China Sea. *Mar. Chem.* **2009**, *117*, 2–10. [CrossRef]
26. Gao, X.; Song, J.; Li, X.; Li, N.; Yuan, H. pCO_2 and carbon fluxes across sea-air interface in the Changjiang Estuary and Hangzhou Bay. *Chin. J. Oceanol. Limnol.* **2008**, *26*, 289–295. [CrossRef]
27. Chou, W.; Gong, G.; Sheu, D.D.; Jan, S.; Huang, C.; Chen, C. Reconciling the paradox that the heterotrophic waters of the East China Sea shelf act as a significant CO_2 sink during the summertime: Evidence and implications. *Geophys. Res. Lett.* **2009**, *36*, 139–156. [CrossRef]
28. Lewis, E.; Wallace, D.; Allison, L.J. *Program Developed for CO_2 System Calculations*; Carbon Dioxide Information Analysis Center, managed by Lockheed Martin Energy Research Corporation for the US Department of Energy Tennessee: Nashville, TN, USA, 1998.
29. Wang, B.; Chen, J.; Jin, H.; Li, H.; Liu, X.; Zhuang, Y.; Xu, Y.; Zhang, H. Preliminary study on the dissolved inorganic carbon system and its response mechanism in Changjiang River Estuary and its adjacent sea areas in summer. *J. Mar. Sci.* **2011**, *29*, 63–70.

30. Zhai, W.; Chen, J.; Jin, H.; Li, H.; Liu, J.; He, X.; Bai, Y. Spring carbonate chemistry dynamics of surface waters in the northern East China Sea: Water mixing, biological uptake of CO_2, and chemical buffering capacity. *J. Geophys. Res. Ocean.* **2015**, *119*, 5638–5653. [CrossRef]
31. Liss, P.S.; Slater, P.G. Flux of gases across the air-sea interface. *Nature* **1974**, *247*, 181–184. [CrossRef]
32. Weiss, R.F. Carbon dioxide in water and seawater: The solubility of a non-ideal gas. *Mar. Chem.* **1974**, *2*, 203–215. [CrossRef]
33. Wanninkhof, R. Relationship between wind speed and gas exchange over the ocean. *J. Geophys. Res.* **1992**, *97*, 7373–7382. [CrossRef]
34. Sweeney, C.; Gloor, E.; Jacobson, A.R.; Key, R.; Mckinley, G.; Sarmiento, J.; Wanninkhof, R. Constraining global air-sea gas exchange for CO_2 with recent bomb ^{14}C measurements. *Glob. Biogeochem. Cycles* **2007**, *21*. [CrossRef]
35. Chaturvedi, M.K.M.; Langote, S.D.; Kumar, D.; Asolekar, S. Significance and estimation of oxygen mass transfer coefficient in simulated waste stabilization pond. *Ecol. Eng.* **2014**, *73*, 331–334. [CrossRef]
36. Nixon, S.W. Physical energy inputs and the comparative ecology of lake and marine ecosystems: Physical energy inputs. *Limnol. Oceanogr.* **1988**, *33*, 1005–1025. [CrossRef]
37. Xue, L.; Cai, W.; Hu, X.; Sabine, C.; Jones, S.; Sutton, A.; Jiang, L.; Reimer, J. Sea surface carbon dioxide at the Georgia time series site (2006–2007): Air–sea flux and controlling processes. *Prog. Oceanogr.* **2016**, *140*, 14–26. [CrossRef]
38. Takahashi, T.; Olafsson, J.; Goddard, J.G.; Chipman, D.; Sutherland, S. Seasonal variation of CO_2 and nutrients in the high-latitude surface oceans: A comparative study. *Glob. Biogeochem. Cycles* **1993**, *7*, 843–878. [CrossRef]
39. Dickson, A.G.; Millero, F.J. A comparison of the equilibrium constants for the dissociation of carbonic acid in seawater media. *Deep Sea Res. Part A Oceanogr. Res. Pap.* **1987**, *34*, 1733–1743. [CrossRef]
40. Sprintall, J.; Tomczak, M. Evidence of the barrier layer in the surface layer of the tropics. *J. Geophys. Res. Ocean.* **1992**, *97*, 7305–7316. [CrossRef]
41. Mehrbach, C.; Culberson, C.H.; Hawley, J.E.; Pytkowicx, R.M. Measurement of the apparent dissociation constants of carbonic acid in seawater at atmospheric pressure. *Limnol. Oceanogr.* **1973**, *18*, 897–907. [CrossRef]
42. Taylor, J.R. *An Introduction to Error Analysis*; University Science Books: Sausalito, CA, USA, 1997.
43. Qu, B.; Song, J.; Li, X.; Yuan, H.; Li, N.; Ma, Q. pCO_2 distribution and CO_2 flux on the inner continental shelf of the East China Sea during summer 2011. *Chin. J. Oceanol. Limnol.* **2013**, *31*, 1088–1097. [CrossRef]
44. Chen, X.; Song, J.; Yuan, H.; Li, X.; Li, N.; Duan, L.; Qu, B. Preliminary study on the change of carbon exchange at sea-air interface and its regional carbon sink intensity in the summer of 2012 in the East China Sea. *Haiyang Xuebao* **2014**, *36*, 18–31.
45. Zhou, F.; Xuan, J.; Ni, X.; Huang, D. Preliminary Analysis of Dynamic Factors of Summer Yangtze River Freshwater Change between 1999 and 2006. *Haiyang Xuebao* **2009**, *31*, 1–12.
46. Milliman, J.D.; Shen, H.; Yang, Z.; Mead, R. Transport and deposition of river sediment in the Changjiang estuary and adjacent continental shelf. *Cont. Shelf Res.* **1985**, *4*, 37–45. [CrossRef]
47. Zhang, J.; Wu, Y.; Jennerjahn, T.C.; Ittekkot, V.; He, Q. Distribution of organic matter in the Changjiang (Yangtze River) Estuary and their stable carbon and nitrogen isotopic ratios: Implications for source discrimination and sedimentary dynamics. *Mar. Chem.* **2007**, *106*, 111–126. [CrossRef]
48. Borges, A.V.; Delille, B.; Frankignoulle, M. Budgeting sinks and sources of CO_2 in the coastal ocean: Diversity of ecosystems counts. *Geophys. Res. Lett.* **2005**, *32*, 301–320. [CrossRef]
49. Cai, W.; Dai, M.; Wang, Y. Air-sea exchange of carbon dioxide in ocean margins: A province-based synthesis. *Geophys. Res. Lett.* **2006**, *33*. [CrossRef]
50. Li, M.; Rong, Z. Effects of tides on freshwater and volume transports in the Changjiang River plume. *J. Geophys. Res. Ocean.* **2012**, *117*. [CrossRef]